Current noise of the interacting resonant level model

T. J. Suzuki,[1] D. M. Kennes,[2] and V. Meden[2]
[1]*Department of Physics, University of Tokyo, Hongo, Tokyo 113-0033, Japan*
[2]*Institut für Theorie der Statistischen Physik, RWTH Aachen University and JARA–Fundamentals of Future Information Technology, 52056 Aachen, Germany*
(Received 1 November 2015; published 4 February 2016)

We study the zero-frequency current noise of the interacting resonant level model for arbitrary bias voltages using a functional renormalization group approach. For this we extend the existing nonequilibrium scheme by deriving and solving flow equations for the current-vertex functions. On-resonance artificial divergences of the latter found in lowest-order perturbation theory in the two-particle interaction are consistently removed. Away from resonance they are shifted to higher orders. This allows us to gain a comprehensive picture of the current noise in the scaling limit. At high bias voltages, the current noise exhibits a universal power-law decay, whose exponent is, to leading order in the interaction, identical to that of the current. The effective charge on resonance is analyzed in detail, employing properties of the vertex correction. We find that it is only modified to second or higher order in the two-particle interaction.

DOI: 10.1103/PhysRevB.93.085306

I. INTRODUCTION

Remarkable advances in nanotechnology open up the possibility to explore transport beyond the linear response regime in experimentally well-controlled situations. Among nanoscale conductors, quantum dot systems have attracted much attention, as they offer a versatile arena in which to study nonequilibrium transport phenomena of interacting fermions. At sufficiently low temperatures, transport is dominated by quantum mechanics. In addition, the local two-particle interaction results in fascinating many-body effects, often accompanied by the emergence of new energy scales. A generic nonequilibrium setup is given by a quantum dot coupled to several leads with different chemical potentials.

The interacting resonant level model (IRLM) is a prominent example in which strong correlations play an essential role [1]. It describes a single-level quantum dot dominated by charge fluctuations which are affected by the local two-particle interaction of dot and lead fermions. The IRLM was originally introduced as a close relative of the Kondo model [1], and, since then, many studies have been performed to elucidate its nonlinear transport properties [2–9]. These have shown that universal features appear in nonequilibrium transport if the lead bandwidth Δ is much larger than any other energy scale. In this scaling regime, the current at large bias voltage is suppressed following a power law, whose exponent depends on the strength of the local interaction [2–4,6–9].

Accumulated knowledge in mesoscopic physics elucidates that the higher order cumulants of the current are of great importance to characterize the nonequilibrium transport [10]. A vast amount of research on the current noise has shown that it contains information which cannot be obtained from conductance measurements, e.g., the effective charge [11–14]. While a unified picture for the current in the IRLM has been established by various methods, the understanding of its higher cumulants is rather limited for the moment. A major obstacle is the absence of a general framework to treat the effects of strong correlations in a nonequilibrium situation. To compute the current noise, one in general needs to consider the current-vertex function [15]. A perturbative approach to the current noise of the IRLM based on the Keldysh technique was put forward in Ref. [16]. Important insights into the noise of the IRLM under on-resonance conditions were gained by utilizing a special symmetry of this model for a particular interaction strength, which is known as self-duality [17]. This symmetry makes it possible to map the IRLM to a solvable boundary sine-Gordon model even in the presence of a driving bias voltage [4]. The effective charge of the quasiparticles of the IRLM at the self-dual point has been investigated using field-theoretical techniques and the density-matrix renormalization group method [18–20]. For the relatively strong interaction at which self-duality is established, the quasiparticles of the IRLM were found to have effective charge $e^* = 2e$ by examining the shot noise [18], which was confirmed computing the full counting statistics [19,20]. This has to be contrasted to $e^* = e$ in the noninteracting limit. In spite of this remarkable achievement, the bias voltage dependence of the current noise of the IRLM away from this self-dual point and off resonance is still an open question. In addition, finite temperature effects were so far not investigated. Considering this situation, it is strongly desirable to develop a systematic framework to calculate the current noise and its full counting statistics in general parameter regimes.

Recently, a functional renormalization group (FRG) method was developed to describe the nonequilibrium properties of correlated fermions [21]. Logarithmic divergences, which manifest themselves in plain perturbation theory even in the equilibrium IRLM, are consistently resummed employing FRG [6]. This method also contributed to deepen our understanding of the nonequilibrium transport properties of the IRLM [6,7]. The renormalization of the hopping between the dot level and the leads can be described using a surprisingly simple approximation [6]. In this paper, we utilize the FRG approach to elucidate the current noise of the nonequilibrium IRLM. In FRG, we can obtain the vertex function by deriving and solving its flow equation. For the level that is on resonance, an artificial divergence of the vertex correction obtained in lowest-order plain perturbation theory in the interaction is removed in the FRG scheme. For off-resonance conditions, a severe divergence, found in perturbation theory if the level

 ©2016 American Physical Society

energy is aligned with one of the lead's chemical potentials, is shifted to higher orders. These achievements allow us to gain a comprehensive picture of the zero-frequency current noise in the scaling limit. We show that the current noise is governed by universal power-law scaling in the large bias voltage regime with an exponent which, to leading order in the interaction, is the same as that of the current. The effective charge is discussed by relating it to the vertex correction. We find that $e^* = e[1 + \mathcal{O}(u^2)]$ with the dimensionless amplitude of the interaction u.

This paper is organized as follows. We describe the model and outline the FRG scheme to compute the current noise in Sec. II. The results for the noise are presented in Sec. III. A summary is given in Sec. IV.

II. MODEL AND FORMALISM

A. Model

The (two-reservoir) IRLM describes a spinless fermionic level coupled to delocalized fermions in the left and right leads. We consider the local repulsion between the fermion in this level and those in both leads. This situation can be modeled by a three-site dot system, in which a particle occupying the central site feels the interaction with the adjacent ones. A schematic picture of the system is shown in Fig. 1(a). The hopping amplitudes $t_{L/R} > 0$ between the three-site dot region and the leads are assumed to be much larger than the intersite ones, such that the lattice sites 1 and 3 are effectively incorporated into the leads. The single-site model studied in the original paper [1] is restored in this limit [6,7,22,23]. The model is described by the action

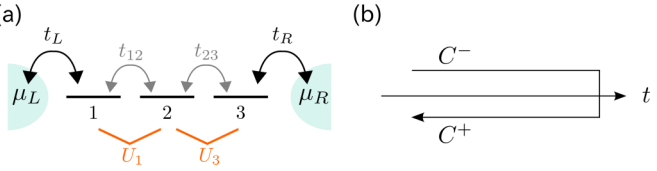

FIG. 1. (a) Schematic picture of the IRLM. (b) The Keldysh contour.

$$S = \sum_{i,j=1}^{3} \int d\tau\, d\tau' \bar{d}_i(\tau) \boldsymbol{g}^{-1}_{dij}(\tau,\tau') d_j(\tau') + \sum_{\alpha=L,R} \sum_{\boldsymbol{k}} \int d\tau\, d\tau' \bar{c}_{\alpha\boldsymbol{k}}(\tau) g^{-1}_{\alpha\boldsymbol{k}}(\tau,\tau') c_{\alpha\boldsymbol{k}}(\tau')$$
$$- \frac{1}{\sqrt{N}} \sum_{\boldsymbol{k}} \int d\tau \left[t_L e^{iA_L(\tau)} \bar{d}_1(\tau) c_{L\boldsymbol{k}}(\tau) + t_R \bar{d}_3(\tau) c_{R\boldsymbol{k}}(\tau) + \text{H.c.} \right] + S_U, \tag{1}$$

where the isolated lead and dot Green's functions are given by $g^{-1}_{\alpha\boldsymbol{k}}(\tau,\tau') \equiv \left[i \frac{d}{d\tau'} - \epsilon_{\alpha\boldsymbol{k}} \right] \delta(\tau,\tau')$ and

$$\boldsymbol{g}^{-1}_d(\tau,\tau') = \begin{pmatrix} i\frac{d}{d\tau'} - (\epsilon_1 - U_1/2) & -t_{12} & 0 \\ -t_{12} & i\frac{d}{d\tau'} - (\epsilon_2 - (U_1+U_3)/2) & -t_{23} \\ 0 & -t_{23} & i\frac{d}{d\tau'} - (\epsilon_3 - U_3/2) \end{pmatrix} \delta(\tau,\tau'), \tag{2}$$

respectively, and the interaction part is given as

$$S_U \equiv - \int d\tau \left[U_1 \bar{d}_2(\tau) d_2(\tau) \bar{d}_1(\tau) d_1(\tau) + U_3 \bar{d}_2(\tau) d_2(\tau) \bar{d}_3(\tau) d_3(\tau) \right]. \tag{3}$$

The argument τ combines the time t and the Keldysh index $\nu = \mp$ [see Fig. 1(b)]. The symbol $\int d\tau$ denotes integration over t and summation over ν. The Grassmann field $\bar{d}_i(\tau)$ [$d_i(\tau)$] creates [annihilates] a spinless fermion at time t, on the Keldysh contour branch with index ν, and on lattice site i. Similarly $\bar{c}_{\alpha\boldsymbol{k}}(\tau)$ [$c_{\alpha\boldsymbol{k}}(\tau)$] is a Grassmann field for creating [annihilating] a fermion in lead α with momentum $\boldsymbol{k}$. The Green's functions in Eq. (1) must be understood as 2×2 matrices in the Keldysh space and the addends contain matrix products which are left implicit. The delta function on the Keldysh contour is defined as $\delta(\tau,\tau') \equiv \delta(t-t')\sigma_z^{\nu\nu'}$ with the standard Pauli matrix σ_z. The energy level of each site is denoted by ϵ_i for $i = 1,2,3$, and the hopping amplitude between the sites 1 (3) and 2 by $t_{12} > 0$ ($t_{23} > 0$). The energy level ϵ_i is defined such that $\epsilon_1 = \epsilon_2 = \epsilon_3 = 0$ corresponds to the particle-hole symmetric case. The third term of the action Eq. (1) describes the hopping between the quantum dot and the leads with N sites. In our expressions we always take the thermodynamic limit $N \to \infty$. The auxiliary vector potential $A_L(\tau)$ is incorporated using the Peierls substitution and later used as a source field to generate the current-vertex function [24]. We choose units with $k_B = 1$, $\hbar = 1$, and elementary charge $e = 1$.

B. Generating functional

The noninteracting reservoirs can be integrated out yielding the action

$$S = \sum_{i,j=1}^{3} \int d\tau\, d\tau' \bar{d}_i(\tau) \boldsymbol{G}^{-1}_{0ij}(\tau,\tau') d_j(\tau') + S_U, \tag{4}$$

where $\boldsymbol{G}_0^{-1}(\tau,\tau') \equiv \boldsymbol{g}_d^{-1}(\tau,\tau') - \boldsymbol{\Sigma}^{-1}_{\text{res}}(\tau,\tau')$. The tunneling self-energy is given as

$$\boldsymbol{\Sigma}_{\text{res}}(\tau,\tau') = \begin{pmatrix} t_L^2 e^{i[A_L(\tau) - A_L(\tau')]} g_L(\tau,\tau') & 0 & 0 \\ 0 & 0 & 0 \\ 0 & 0 & t_R^2 g_R(\tau,\tau') \end{pmatrix}, \tag{5}$$

with $g_\alpha(\tau,\tau') = \frac{1}{N} \sum_{\boldsymbol{k}} g_{\alpha\boldsymbol{k}}(\tau,\tau')$. We consider the system with a time-independent bias voltage V, which is applied

symmetrically to the leads, i.e., $\mu_L = V/2$ and $\mu_R = -V/2$. Both of the leads are assumed to be in equilibrium. Since in its bias-voltage-driven nonequilibrium steady state the system is invariant under time translation, we perform a Fourier transform to energy representation.

As usual in the Keldysh formalism we use the representation with the retarded (r), Keldysh (K), and advanced (a) components instead of the one with $\nu = \mp$ if appropriate. The component which vanishes in the two-point Green's function due to causality but appears for other vertices (see below) is denoted by $\tilde{K}$. If the source field $A_L(\tau)$ is set to be zero, the relevant parts of the tunneling self-energy are obtained as

$$\mathbf{\Sigma}^{\mathrm{r}}_{\mathrm{res}}(\omega) = \begin{pmatrix} -\frac{i\Delta_L}{2} & 0 & 0 \\ 0 & 0 & 0 \\ 0 & 0 & -\frac{i\Delta_R}{2} \end{pmatrix}, \tag{6}$$

$$\mathbf{\Sigma}^{\mathrm{K}}_{\mathrm{res}}(\omega) = \begin{pmatrix} i\Delta_L(2f_L(\omega)-1) & 0 & 0 \\ 0 & 0 & 0 \\ 0 & 0 & i\Delta_R(2f_R(\omega)-1) \end{pmatrix}. \tag{7}$$

Here, we use the wide-band limit and define the bandwidth, $\Delta_\alpha \equiv 2\pi\rho_\alpha t_\alpha^2$. For simplicity, we assume $\Delta_L = \Delta_R \equiv \Delta$, $t_{12} = t_{23} \equiv t$, $\epsilon_1 = \epsilon_3 = 0$, $\epsilon_2 = \epsilon$, and $U_1 = U_3 \equiv U \geqslant 0$. This implies that at particle-hole symmetry $\epsilon = 0$ transport is resonant. We thus refer to this case either as the particle-hole symmetric point or the on-resonance situation.

Following the standard functional integral approach to quantum many-body physics [24], we introduce the additional source term

$$S^{\mathrm{s}} \equiv \sum_{i=1}^{3} \int d\tau [\bar{\eta}_i(\tau) d_i(\tau) + \bar{d}_i(\tau)\eta_i(\tau)], \tag{8}$$

which allows us to generate correlation functions by functional derivatives. The corresponding generating functional is given by

$$W[\eta,\bar{\eta},A] \equiv -i \ln \int \mathcal{D}[\bar{d},d] \exp[i(S+S^{\mathrm{s}})]. \tag{9}$$

The effective action [25] is defined using the Legendre transform as

$$\Gamma[\langle d\rangle^{\mathrm{s}},\langle\bar{d}\rangle^{\mathrm{s}},A] \equiv W[\eta,\bar{\eta},A] - \sum_{i=1}^{3} \int d\tau [\bar{\eta}_i(\tau)\langle d_i\rangle^{\mathrm{s}}(\tau) + \langle\bar{d}_i\rangle^{\mathrm{s}}(\tau)\eta_i(\tau)], \tag{10}$$

with

$$\langle\mathcal{O}\rangle^{\mathrm{s}} \equiv \frac{\int \mathcal{D}[\bar{d},d]\mathcal{O}\exp[i(S+S^{\mathrm{s}})]}{\int \mathcal{D}[\bar{d},d]\exp[i(S+S^{\mathrm{s}})]}. \tag{11}$$

This effective action acts as the generating functional of one-particle irreducible vertex functions (e.g., the self-energy). The vertex expansion of the effective action is given as

$$\begin{aligned}\Gamma[\langle d\rangle^{\mathrm{s}},\langle\bar{d}\rangle^{\mathrm{s}},A] &= \sum_{m,n=0}^{\infty} \frac{(-1)^m}{(m!)^2}\frac{1}{n!} \prod_{j,k=0}^{m}\prod_{l=0}^{n} \int d\tau_j d\tau'_k d\tau''_l\, \gamma^{(2m,n)}_{i'_1\cdots i'_m;i_1\cdots i_m;\alpha_1\cdots\alpha_n} \\ &\times (\tau'_1,\ldots,\tau'_m;\tau_1,\ldots,\tau_m;\tau''_1,\ldots,\tau''_n)\langle\bar{d}_{i'_1}\rangle^{\mathrm{s}}(\tau'_1)\cdots \\ &\times \langle\bar{d}_{i'_m}\rangle^{\mathrm{s}}(\tau'_m)\langle d_{i_1}\rangle^{\mathrm{s}}(\tau_1)\cdots\langle d_{i_m}\rangle^{\mathrm{s}}(\tau_m)A_{\alpha_1}(\tau''_1)\cdots A_{\alpha_n}(\tau''_n),\end{aligned} \tag{12}$$

where repeated site indices are summed over. We note that the auxiliary vector potential $A_\alpha(\tau)$ is also defined on the Keldysh contour; i.e., it has the two components $A^-_\alpha(t)$ and $A^+_\alpha(t)$. Hence, there are in total 2^{2m+n} components for the current-vertex function $\gamma^{(2m,n)}$.

The doubled degrees of freedom of the vector potential allow one to completely describe both the dynamical evolution as well as the statistical correlation [24,25]. We define the source and the physical component of the vector potential as

$$A^{\mathrm{s}}_\alpha(t) \equiv \tfrac{1}{2}\big[A^-_\alpha(t) - A^+_\alpha(t)\big], \quad A^{\mathrm{p}}_\alpha(t) \equiv \tfrac{1}{2}\big[A^-_\alpha(t) + A^+_\alpha(t)\big], \tag{13}$$

respectively. We utilize $A^{\mathrm{s}}(t)$ to derive the expression of the current-vertex functions and their flow equations. After deriving all the equations, we take the physically relevant limit $A^{\mathrm{s}}(t) \to 0$. As we introduced the bias voltage via the chemical potentials of the leads and do not consider any further fields, the physical component of the vector potential is set to zero as well. The source and physical components of the current-vertex functions are defined as

$$(\gamma^{(0,1)})^{\mathrm{s}}_\alpha(t) \equiv \left.\frac{\delta\Gamma}{\delta A^{\mathrm{s}}_\alpha(t)}\right|_{A^{\mp}_\alpha=0}, \quad (\gamma^{(0,1)})^{\mathrm{p}}_\alpha(t) \equiv \left.\frac{\delta\Gamma}{\delta A^{\mathrm{p}}_\alpha(t)}\right|_{A^{\mp}_\alpha=0}, \tag{14}$$

respectively. The components of the higher order current-vertex functions are defined in the same way. Then, the current noise can be written as [26]

$$\begin{aligned}S_{\alpha\alpha'}(t,t') &\equiv \langle I_\alpha(t)I_{\alpha'}(t')\rangle + \langle I_{\alpha'}(t')I_\alpha(t)\rangle - 2\langle I_\alpha(t)\rangle\langle I_{\alpha'}(t')\rangle \\ &= S^0_{\alpha\alpha'}(t,t') + S^U_{\alpha\alpha'}(t,t'),\end{aligned} \tag{15}$$

where the two terms are defined as

$$\begin{aligned}S^0_{\alpha\alpha'}(t,t') \equiv{}& \frac{1}{2}\int dt_1 dt'_1 \boldsymbol{G}^{\nu_1\nu'_1}_{i_1 i'_1}(t_1,t'_1)\sigma_z^{\nu'_1\nu'_1}\big(\boldsymbol{\gamma}^{(2,2)}_{\mathrm{res}}\big)^{\nu'_1\nu_1;\mathrm{ss}}_{i'_1 i_1;\alpha\alpha'}(t'_1,t_1;t,t')\sigma_z^{\nu_1\nu_1} \\ &+ \frac{1}{2}\int dt_1 dt_2 dt'_1 dt'_2 \boldsymbol{G}^{\nu_2\nu'_1}_{i_2 i'_1}(t_2,t'_1)\sigma_z^{\nu'_1\nu'_1}\big(\boldsymbol{\gamma}^{(2,1)}_{\mathrm{res}}\big)^{\nu'_1\nu_1;\mathrm{s}}_{i'_1 i_1;\alpha}(t'_1,t_1;t)\sigma_z^{\nu_1\nu_1}\boldsymbol{G}^{\nu_1\nu'_2}_{i_1 i'_2}(t_1,t'_2)\sigma_z^{\nu'_2\nu'_2}\big(\boldsymbol{\gamma}^{(2,1)}_{\mathrm{res}}\big)^{\nu'_2\nu_2;\mathrm{s}}_{i'_2 i_2;\alpha'}(t'_2,t_2;t')\sigma_z^{\nu_2\nu_2},\end{aligned} \tag{16}$$

$$S^U_{\alpha\alpha'}(t,t') \equiv \frac{1}{2}\int dt_1 dt_2 dt'_1 dt'_2 \boldsymbol{G}^{\nu_2\nu'_1}_{i_2 i'_1}(t_2,t'_1)\sigma_z^{\nu'_1\nu'_1}(\bar{\boldsymbol{\gamma}}^{(2,1)})^{\nu'_1\nu_1;\mathrm{s}}_{i'_1 i_1;\alpha}(t'_1,t_1;t)\sigma_z^{\nu_1\nu_1}\boldsymbol{G}^{\nu_1\nu'_2}_{i_1 i'_2}(t_1,t'_2)\sigma_z^{\nu'_2\nu'_2}\big(\boldsymbol{\gamma}^{(2,1)}_{\mathrm{res}}\big)^{\nu'_2\nu_2;\mathrm{s}}_{i'_2 i_2;\alpha'}(t'_2,t_2;t')\sigma_z^{\nu_2\nu_2}, \tag{17}$$

FIG. 2. Diagrammatic representation of the current noise. The circle represents the three-point vertex function. The left diagram is called the bubble term, while the right is called the vertex correction.

with

$$(\bar{\boldsymbol{\gamma}}^{(2,1)})^{\nu_1'\nu_1;\mathrm{s}}_{i_1'i_1;\alpha}(t_1',t_1;t) \equiv (\boldsymbol{\gamma}^{(2,1)})^{\nu_1'\nu_1;\mathrm{s}}_{i_1'i_1;\alpha}(t_1',t_1;t) - \left(\boldsymbol{\gamma}^{(2,1)}_{\mathrm{res}}\right)^{\nu_1'\nu_1;\mathrm{s}}_{i_1'i_1;\alpha}(t_1',t_1;t). \quad (18)$$

Here, $\gamma^{(2,n)}_{\mathrm{res}}$ (for $n > 0$) is the noninteracting part of the $(2+n)$-point current-vertex function. Thus $\bar{\boldsymbol{\gamma}}^{(2,1)}$ defined in Eq. (18) is the interaction induced part of the three-point vertex function. In Eqs. (16) and (17) the repeated Keldysh indices $\nu = \mp$ and site indices are summed over. The first term S^0 on the right-hand side of Eq. (15) is called the bubble term, while the second S^U is the vertex correction to the noise. Their diagrammatic representations are shown in Fig. 2. The effect of the repulsive interaction is included in the self-energy of the propagator, $\boldsymbol{\Sigma}_U = \boldsymbol{G}_0^{-1} - \boldsymbol{\gamma}^{(2,0)}$, and the three-point vertex function, $\gamma^{(2,1)}$, both being determined by the FRG approach.

C. Functional renormalization group approach

In setting up the functional renormalization group approach [21], we use a reservoir cutoff as the flow parameter [22,23]. The Kubo-Martin-Schwinger (KMS) condition is automatically preserved in this scheme, which is important to perform calculations consistent with the fluctuation dissipation theorem in the limit $V \to 0$. The flow parameter is introduced as an additional tunneling self-energy,

$$\boldsymbol{\Sigma}^{\mathrm{r}}_{\mathrm{aux},\Lambda}(\omega) = -\frac{i\Lambda}{2}\mathbf{1}, \quad (19)$$

$$\boldsymbol{\Sigma}^{\mathrm{K}}_{\mathrm{aux},\Lambda}(\omega) = i\Lambda[2f_{\mathrm{aux}}(\omega) - 1]\mathbf{1}, \quad (20)$$

where $f_{\mathrm{aux}}(\omega)$ is the Fermi-Dirac distribution function of the auxiliary structureless reservoirs and $\mathbf{1}$ is the identity matrix of dimension 3. It was examined earlier that results for the current are independent of the choice of the temperature in the auxiliary reservoirs [27,28]. In this paper, we utilize the auxiliary reservoirs with infinite temperature and thus $f_{\mathrm{aux}}(\omega) = 1/2$. This simplifies the flow equations as the Keldysh component of the auxiliary self-energy vanishes. The full Green's function is obtained by the Dyson equation:

$$\left(\boldsymbol{G}^{\mathrm{r}}_{\Lambda}\right)^{-1}(\omega) = \left(\boldsymbol{G}^{\mathrm{r}}_{0}\right)^{-1}(\omega) - \boldsymbol{\Sigma}^{\mathrm{r}}_{\mathrm{aux},\Lambda}(\omega) - \boldsymbol{\Sigma}^{\mathrm{r}}_{U,\Lambda}(\omega), \quad (21)$$

$$\left(\boldsymbol{G}^{\mathrm{K}}_{\Lambda}\right)(\omega) = \boldsymbol{G}^{\mathrm{r}}_{\Lambda}(\omega)\left[\boldsymbol{\Sigma}^{\mathrm{K}}_{\mathrm{res}}(\omega) + \boldsymbol{\Sigma}^{\mathrm{K}}_{U,\Lambda}(\omega)\right]\boldsymbol{G}^{\mathrm{a}}_{\Lambda}(\omega). \quad (22)$$

The scale-dependent propagator $\boldsymbol{S}_\Lambda(\tau,\tau')$ appearing in the RG flow equations (see below) is defined as

$$\boldsymbol{S}_\Lambda(\tau,\tau') \equiv \int d\tau_1 d\tau_2 \boldsymbol{G}_\Lambda(\tau,\tau_1)\frac{d\boldsymbol{\Sigma}_{\mathrm{aux},\Lambda}(\tau_1,\tau_2)}{d\Lambda}\boldsymbol{G}_\Lambda(\tau_2,\tau'). \quad (23)$$

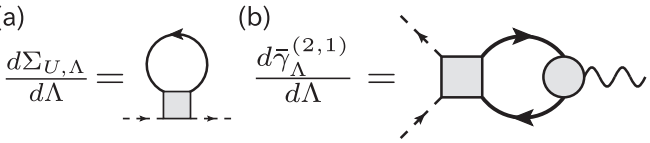

FIG. 3. Diagrammatic representation of the flow equations of (a) the self-energy and (b) the three-point current-vertex function in the static approximation. The square represents the two-particle interaction.

with components

$$\boldsymbol{S}^{\mathrm{r}}_{\Lambda}(\omega) = \frac{-i}{2}\boldsymbol{G}^{\mathrm{r}}_{\Lambda}(\omega)\boldsymbol{G}^{\mathrm{r}}_{\Lambda}(\omega), \quad (24)$$

$$\boldsymbol{S}^{\mathrm{K}}_{\Lambda}(\omega) = \frac{-i}{2}\boldsymbol{G}^{\mathrm{r}}_{\Lambda}(\omega)\boldsymbol{G}^{\mathrm{K}}_{\Lambda}(\omega) + \frac{i}{2}\boldsymbol{G}^{\mathrm{K}}_{\Lambda}(\omega)\boldsymbol{G}^{\mathrm{a}}_{\Lambda}(\omega). \quad (25)$$

We consider the model with $\Lambda_{\mathrm{init}} \to \infty$ as the initial one of the flow, as all the vertex functions can be calculated exactly in this limit. The initial conditions of the self-energy and the vertex functions are summarized in Appendix A. The set of coupled flow equations has to be integrated down to $\Lambda = 0$, at which the auxiliary reservoirs are decoupled and the cutoff-free problem of interest is restored.

In order to implement numerical calculations, we need to truncate the infinite hierarchy of the flow equations to a given order. In this paper, we use the lowest order truncation, which is known as the static approximation [21], to determine the flow equations of the self-energy and current-vertex functions. Flow equations are truncated at the first order in the interaction, U. The remaining terms are the Hartree-Fock-type diagram for the self-energy—we note that due to the underlying RG procedure our approximation is not equivalent to the Hartree-Fock approximation—and the RPA-type diagram for the vertex function. The diagrammatic representation of the flow equations is given in Fig. 3. In spite of this simple treatment, this approximation for the self-energy is known to describes the rich properties of nonequilibrium transport due to the built-in renormalization [21]. In particular, logarithmic divergences found in the scaling limit of the IRLM in plain perturbation theory are consistently resummed to power laws [6]. The current-vertex function has not yet been treated within the present truncated FRG scheme, and its role for the current noise is discussed below. We note that higher order corrections can be systematically included in principle by incorporating flow equations of higher order vertices.

The flow equation of the four-point vertex function is ignored in the static approximation, and its value is replaced by the initial one which is given by the anti-symmetrized bare two-particle interaction $U_{ik;jl}$ (see Appendix A).

The flow equation of the self-energy is obtained as (repeated site indices are summed over)

$$\frac{d}{d\Lambda}\left(\boldsymbol{\Sigma}^{\mathrm{r}}_{U,\Lambda}\right)_{ij} = \frac{iU_{ik;jl}}{2}\int\frac{d\omega}{2\pi}\left(\boldsymbol{S}^{\mathrm{K}}_{\Lambda}\right)_{lk}(\omega). \quad (26)$$

Within the present approximation, the self-energy is frequency independent due to the structure of the right-hand side. Hence, single-particle Green's functions can be interpreted as effective noninteracting ones with renormalized parameters.

The flow equation of the retarded component of the interaction-induced part of the three-point vertex function [see Eq. (18)] is given by

$$\frac{d}{d\Lambda}\left(\bar{\boldsymbol{\gamma}}_\Lambda^{(2,1)}\right)^{\mathrm{r;s}}_{ij;L} = \frac{iU_{ik;jl}}{2}\left[\left(\boldsymbol{\Phi}_\Lambda^{(2,1)}\right)^{\mathrm{K}}_{lk} + \left(\boldsymbol{\Phi}_\Lambda^{(2,1)}\right)^{\tilde{\mathrm{K}}}_{lk}\right], \tag{27}$$

with

$$\begin{aligned}\left(\boldsymbol{\Phi}_\Lambda^{(2,1)}\right)^{\mathrm{K}} \equiv \int \frac{d\omega}{2\pi}\Big[&\boldsymbol{S}^{\mathrm{r}}_\Lambda(\omega)\left(\boldsymbol{\gamma}_\Lambda^{(2,1)}\right)^{\mathrm{r;s}}_{;L}\boldsymbol{G}^{\mathrm{K}}_\Lambda(\omega) + \boldsymbol{S}^{\mathrm{K}}_\Lambda \\ &\times(\omega)\left(\boldsymbol{\gamma}_\Lambda^{(2,1)}\right)^{\mathrm{a;s}}_{;L}\boldsymbol{G}^{\mathrm{a}}_\Lambda(\omega) + \boldsymbol{S}^{\mathrm{r}}_\Lambda(\omega)\left(\boldsymbol{\gamma}_\Lambda^{(2,1)}\right)^{\mathrm{K;s}}_{;L}\boldsymbol{G}^{\mathrm{a}}_\Lambda(\omega) \\ &+ \boldsymbol{S}^{\mathrm{K}}_\Lambda(\omega)\left(\boldsymbol{\gamma}_\Lambda^{(2,1)}\right)^{\tilde{\mathrm{K}};\mathrm{s}}_{;L}\boldsymbol{G}^{\mathrm{K}}_\Lambda(\omega) + (\boldsymbol{S}\leftrightarrow\boldsymbol{G})\Big],\end{aligned} \tag{28}$$

and

$$\left(\boldsymbol{\Phi}_\Lambda^{(2,1)}\right)^{\tilde{\mathrm{K}}} \equiv \int \frac{d\omega}{2\pi}\Big[\boldsymbol{S}^{\mathrm{a}}_\Lambda(\omega)\left(\boldsymbol{\gamma}_\Lambda^{(2,1)}\right)^{\tilde{\mathrm{K}};s}_{;L}\boldsymbol{G}^{\mathrm{r}}_\Lambda(\omega) + (\boldsymbol{S}\leftrightarrow\boldsymbol{G})\Big]. \tag{29}$$

The abbreviation $(\boldsymbol{S}\leftrightarrow\boldsymbol{G})$ denotes the terms which are obtained by mutually replacing $\boldsymbol{S}$ and $\boldsymbol{G}$ in the preceding ones in the same parenthesis. Similarly, the flow equation of the Keldysh component is obtained as

$$\frac{d}{d\Lambda}\left(\bar{\boldsymbol{\gamma}}_\Lambda^{(2,1)}\right)^{\mathrm{K;s}}_{ij;L} = \frac{iU_{ik;jl}}{2}\left[\left(\boldsymbol{\Phi}_\Lambda^{(2,1)}\right)^{\mathrm{r}}_{lk} + \left(\boldsymbol{\Phi}_\Lambda^{(2,1)}\right)^{\mathrm{a}}_{lk}\right], \tag{30}$$

with

$$\begin{aligned}\left(\boldsymbol{\Phi}_\Lambda^{(2,1)}\right)^{\mathrm{r}} \equiv \int \frac{d\omega}{2\pi}\Big[&\boldsymbol{S}^{\mathrm{r}}_\Lambda(\omega)\left(\boldsymbol{\gamma}_\Lambda^{(2,1)}\right)^{\mathrm{r;s}}_{;L}\boldsymbol{G}^{\mathrm{r}}_\Lambda(\omega) \\ &+ \boldsymbol{S}^{\mathrm{K}}_\Lambda(\omega)\left(\boldsymbol{\gamma}_\Lambda^{(2,1)}\right)^{\tilde{\mathrm{K}};\mathrm{s}}_{;L}\boldsymbol{G}^{\mathrm{r}}_\Lambda(\omega) + (\boldsymbol{S}\leftrightarrow\boldsymbol{G})\Big],\end{aligned} \tag{31}$$

and

$$\begin{aligned}\left(\boldsymbol{\Phi}_\Lambda^{(2,1)}\right)^{\mathrm{a}} \equiv \int \frac{d\omega}{2\pi}\Big[&\boldsymbol{S}^{\mathrm{a}}_\Lambda(\omega)\left(\boldsymbol{\gamma}_\Lambda^{(2,1)}\right)^{\mathrm{a;s}}_{;L}\boldsymbol{G}^{\mathrm{a}}_\Lambda(\omega) \\ &+ \boldsymbol{S}^{\mathrm{a}}_\Lambda(\omega)\left(\boldsymbol{\gamma}_\Lambda^{(2,1)}\right)^{\tilde{\mathrm{K}};\mathrm{s}}_{;L}\boldsymbol{G}^{\mathrm{K}}_\Lambda(\omega) + (\boldsymbol{S}\leftrightarrow\boldsymbol{G})\Big].\end{aligned} \tag{32}$$

Again, repeated site indices are summed over. The argument of the three-point vertex functions is omitted as these turn out to be independent of frequency in the static approximation. In contrast to the self-energy, these vertex functions do not have a simple interpretation in reference to a noninteracting model.

Using the initial condition and the flow equation, we can prove that the three-point current-vertex functions fulfill the symmetry relations

$$\left[\left(\boldsymbol{\gamma}_\Lambda^{(2,1)}\right)^{\mathrm{r;s}}_{ij;L}\right]^* = -\left(\boldsymbol{\gamma}_\Lambda^{(2,1)}\right)^{\mathrm{a;s}}_{ji;L}, \tag{33}$$

$$\left[\left(\boldsymbol{\gamma}_\Lambda^{(2,1)}\right)^{\mathrm{K;s}}_{ij;L}\right]^* = \left(\boldsymbol{\gamma}_\Lambda^{(2,1)}\right)^{\mathrm{K;s}}_{ji;L}, \tag{34}$$

$$\left[\left(\boldsymbol{\gamma}_\Lambda^{(2,1)}\right)^{\tilde{\mathrm{K}};\mathrm{s}}_{ij;L}\right]^* = \left(\boldsymbol{\gamma}_\Lambda^{(2,1)}\right)^{\tilde{\mathrm{K}};\mathrm{s}}_{ji;L}. \tag{35}$$

In the static approximation, we can derive the additional relations

$$\left(\bar{\boldsymbol{\gamma}}_\Lambda^{(2,1)}\right)^{\mathrm{r;s}}_{ij;L} = \left(\bar{\boldsymbol{\gamma}}_\Lambda^{(2,1)}\right)^{\mathrm{a;s}}_{ji;L}, \tag{36}$$

$$\left(\bar{\boldsymbol{\gamma}}_\Lambda^{(2,1)}\right)^{\mathrm{K;s}}_{ij;L} = \left(\bar{\boldsymbol{\gamma}}_\Lambda^{(2,1)}\right)^{\tilde{\mathrm{K}};\mathrm{s}}_{ij;L}. \tag{37}$$

Hence, it is sufficient to determine the retarded and the Keldysh component of the three-point vertex function.

We determine the self-energy and the three-point current-vertex functions by solving these flow equations numerically, and use the $\Lambda = 0$ functions in the formula of the current noise given in Eqs. (15)–(18). Details of the numerical implementation are given in Appendix B.

III. RESULTS

A. A consistency check for the current

There have already been an extensive number of studies on the steady-state current of the IRLM to elucidate its rich properties [2–9]. We here focus on the case of the bandwidth Δ being much larger than the other energy scales of the problem. It is known as the scaling limit, and universal features of the steady-state current, such as the power-law behavior at large bias voltages, manifest themselves [2–4,6–9]. In an earlier FRG approach, the current was computed from the self-energy employing the Meir-Wingreen formula [29]. In this subsection, it is discussed that an alternative FRG formulation can be developed in which a flow equation for the current is derived and solved. We show that both schemes provide the same results up to linear order in U, which is the one to which our truncation is controlled. As the flowing current-vertex functions derived above enter the flow equation for the current this provides a nontrivial consistency-check of our formulation later used to study the noise.

The explicit expression of the current using the Meir-Wingreen formula is given as

$$\begin{aligned}I^{\mathrm{MW}}_\Lambda = \frac{1}{2\pi}\int d\omega\big[&T^\Lambda_{LR}(\omega)(f_L(\omega) - f_R(\omega)) \\ &+ T^\Lambda_{L\mathrm{aux}}(\omega)(f_L(\omega) - f_{\mathrm{aux}}(\omega))\big],\end{aligned} \tag{38}$$

with

$$T^\Lambda_{LR}(\omega) = \Delta_L\Delta_R\left(\boldsymbol{G}^{\mathrm{r}}_\Lambda\right)_{13}(\omega)\left(\boldsymbol{G}^{\mathrm{a}}_\Lambda\right)_{31}(\omega), \tag{39}$$

$$T^\Lambda_{L\mathrm{aux}}(\omega) = \Delta_L\Lambda\left(\boldsymbol{G}^{\mathrm{r}}_\Lambda\boldsymbol{G}^{\mathrm{a}}_\Lambda\right)_{11}(\omega). \tag{40}$$

This should be equivalent to the current obtained by solving its flow equation, which is denoted by $I^{\mathrm{flow}}_\Lambda$. If we focus on their difference, i.e., $\bar{I}_\Lambda \equiv I^{\mathrm{MW}}_\Lambda - I^{\mathrm{flow}}_\Lambda$, its flow equation is given by

$$\begin{aligned}\frac{d\bar{I}_\Lambda}{d\Lambda} = &\frac{-i}{2}\int\frac{d\omega}{2\pi}(\boldsymbol{S}_\Lambda)^{\mathrm{r}}_{ij}(\omega)\left(\bar{\boldsymbol{\gamma}}_\Lambda^{(2,1)}\right)^{\mathrm{r;s}}_{ji;L}(\omega;\omega;0) \\ &- \frac{i}{2}\int\frac{d\omega}{2\pi}(\boldsymbol{S}_\Lambda)^{\mathrm{a}}_{ij}(\omega)\left(\bar{\boldsymbol{\gamma}}_\Lambda^{(2,1)}\right)^{\mathrm{a;s}}_{ji;L}(\omega;\omega;0) \\ &- \frac{i}{2}\int\frac{d\omega}{2\pi}(\boldsymbol{S}_\Lambda)^{\mathrm{K}}_{ij}(\omega)\left(\bar{\boldsymbol{\gamma}}_\Lambda^{(2,1)}\right)^{\tilde{\mathrm{K}};\mathrm{s}}_{ji;L}(\omega;\omega;0) \\ &+ \frac{i}{2}\Delta_L\int\frac{d\omega}{2\pi}\Bigg((2f_L(\omega)-1)\Bigg[\left(\boldsymbol{G}^{\mathrm{r}}_\Lambda\frac{d\boldsymbol{\Sigma}^{\mathrm{r}}_U}{d\Lambda}\boldsymbol{G}^{\mathrm{r}}_\Lambda\right. \\ &\left.- \boldsymbol{G}^{\mathrm{a}}_\Lambda\frac{d\boldsymbol{\Sigma}^{\mathrm{a}}_U}{d\Lambda}\boldsymbol{G}^{\mathrm{a}}_\Lambda\right)_{11}(\omega)\Bigg]\left(\boldsymbol{G}^{\mathrm{r}}_\Lambda\frac{d\boldsymbol{\Sigma}^{\mathrm{r}}_U}{d\Lambda}\boldsymbol{G}^{\mathrm{K}}_\Lambda\right)_{11}(\omega) \\ &- \left(\boldsymbol{G}^{\mathrm{K}}_\Lambda\frac{d\boldsymbol{\Sigma}^{\mathrm{a}}_U}{d\Lambda}\boldsymbol{G}^{\mathrm{a}}_\Lambda\right)_{11}(\omega)\Bigg),\end{aligned} \tag{41}$$

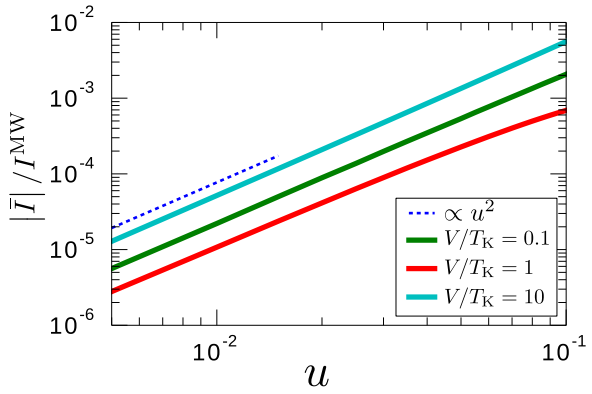

FIG. 4. The dependence of $\bar{I}$ on the dimensionless interaction u for various V. The unit of energy, T_{K}, is introduced in Sec. III B. The parameters are $t/\Delta = 0.001$, $\epsilon/T_{\mathrm{K}} = 0$, and $T/T_{\mathrm{K}} = 0$.

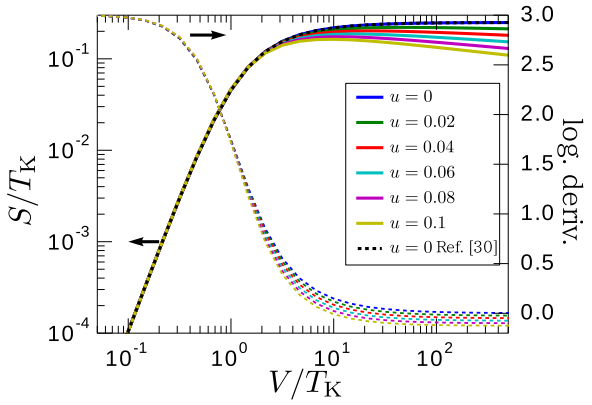

FIG. 5. The dependence of noise and its logarithmic derivative on V for various u. The parameters are $\epsilon/T_{\mathrm{K}} = 0$, $t/\Delta = 0.001$, and $T/T_{\mathrm{K}} = 0$.

with initial condition $\bar{I}_{\Lambda_{\mathrm{init}}} = 0$. As mentioned above, it contains the flowing current-vertex function $\bar{\gamma}^{(2,1)}_{\Lambda}$. The right-and side is zero if the infinite hierarchy of flow equations is kept, but may become finite if we use approximations, e.g., the static one.

Equation (41) together with the expression for the self-energy Eq. (26) as well as the vertex functions Eqs. (27) and (30) can be solved numerically. The resulting value of the relative difference, $|\bar{I}|/I^{\mathrm{MW}}$ as a function of the dimensionless interaction $u \equiv U/\Delta$ is plotted in Fig. 4. Within the static approximation the difference should be of second order in u, i.e., $\bar{I} \equiv \bar{I}_{\Lambda=0} = \mathcal{O}(u^2)$, which is consistent with the results shown in Fig. 4 for various V. This finding indicates that we can consistently determine the current by solving its flow equation and that the flow of the current-vertex function was properly implemented. As briefly discussed in the next section, which is mainly on the noise, we can reproduce all the known results for the current, e.g., power-law scaling with a U-dependent exponent at large voltages from $I^{\mathrm{flow}}_{\Lambda}$.

B. On-resonance current noise

It was established by previous works that the low-energy physics of the IRLM is governed by a single energy scale, T_{K} (see, e.g., Ref. [6]). Here this universal energy scale is introduced as $T_{\mathrm{K}} \equiv 8|\bar{t}^{\mathrm{ren}}|^2/\Delta$ with the renormalized hopping amplitude $\bar{t}^{\mathrm{ren}} \equiv t + \Sigma^{\mathrm{r}}_{12}|_{T=V=\epsilon=0}$ at the end of the RG flow. An alternative definition using the susceptibility is discussed in Appendix C. The current shows a crossover from the linear response regime to power-law decay [4,6] at $V \simeq T_{\mathrm{K}}$. Hence, it is natural to expect T_{K} as the characteristic energy scale of the current noise as well. It is sufficient to focus on the component $S \equiv S_{LL}(\omega = 0)$ due to the charge conservation. In this subsection we consider the transport on resonance with $\epsilon = 0$.

The dependence of the temperature $T = 0$ zero-frequency current noise obtained by numerically solving the flow equations (for details of the implementation see Appendix B) on the bias voltage V is shown in Fig. 5 for various u. The logarithmic derivative $d\ln[S(V)]/d\ln(V)$, approximated by centered differences, is shown in the same figure. If $S(V)$ is governed by power-law behavior, the exponent can be read off from the plateau value of this quantity. From this, it is evident that $S(V)$ is proportional to V^3 for small V. The curves for the current noise collapse into a single one in the linear response regime ($V \leqslant T_{\mathrm{K}}$) if properly scaled by T_{K}. This indicates that the prefactor of the leading $(V/T_{\mathrm{K}})^3$ behavior of the noise is independent of the two-particle interaction. For $u = 0$ the noise computed by FRG agrees with the analytic expression given in Ref. [30]. The latter is shown as the thick dashed line in Fig. 5.

It is well established that the $T = 0$ current shows power-law suppression at high bias voltages,

$$I/T_{\mathrm{K}} \sim (V/T_{\mathrm{K}})^{\alpha_I}, \tag{42}$$

with an interaction-dependent exponent which to leading order in u is given by

$$\alpha_I = -\frac{4u}{\pi}. \tag{43}$$

The constant logarithmic derivative at large bias voltages in Fig. 5 indicates that the current noise exhibits power-law behavior in the same regime as well:

$$S/T_{\mathrm{K}} \sim (V/T_{\mathrm{K}})^{\alpha_S}. \tag{44}$$

The logarithmic derivatives of the current and noise are compared in Fig. 6. The dashed lines in Fig. 6(a) and the solid line in Fig. 6(b) indicate the exponent Eq. (43). For the current, this value can be obtained analytically using FRG [6]. The logarithmic derivative of the noise is found to reach the same value as that of the current at sufficiently large bias voltages. Previous works employing FRG showed that the behavior of the current can be understood from an effective noninteracting model with renormalized parameters, in particular a renormalized level-lead hopping [6]. As the current-vertex corrections enter the expression for the noise, it is not obvious that a similar mapping can be used for the noise. The contribution of the vertex correction to the current noise is discussed in more detail in the next section.

We show plots of the noise as a function of V for various temperatures in Fig. 7. The black dashed lines in Fig. 7(a) are the thermal noise calculated via the fluctuation-dissipation theorem $S_{\mathrm{th}} = 4GT$ for each temperature with the linear conductance defined (and numerically computed) as

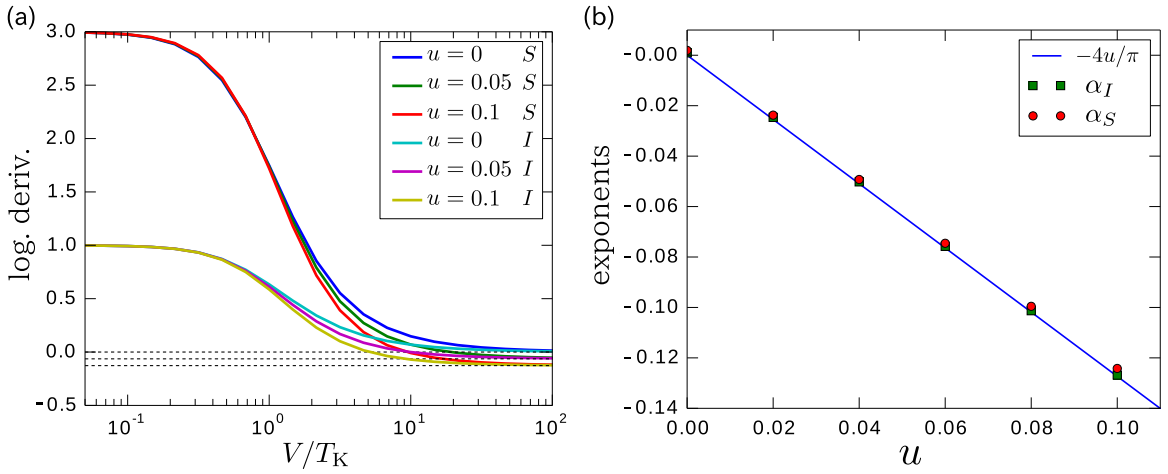

FIG. 6. (a) The dependence of the logarithmic derivative of the current and noise on V for various u. (b) The exponents at large bias voltages for various u. The parameters are $\epsilon/T_K = 0$, $t/\Delta = 0.001$, and $T/T_K = 0$.

$G \equiv dI/dV|_{V=0}$. The excellent agreement confirms that the current noise obeys the fluctuation dissipation relation in the zero-bias limit, $S(V/T_K \to 0) = 4GT$. The crossover from thermal to shot noise occurs around voltages which fulfill $S_3V^3 \sim TG$, where S_3 is the coefficient of the V^3 term in the current noise S. The independence of the coefficient S_3 on u in the low-bias regime is discussed later in detail. The power-law behavior at large voltages is observed for temperatures sufficiently lower than T_K. The current noise calculated at temperatures larger than T_K is shown in Fig. 7(b). The power-law decay at high bias voltages survives even in this limit if the bias voltage is larger than T. In other words, the current noise exhibits power-law decay at sufficiently large voltages which satisfy $V \gg \max\{T, T_K\}$. Due to this renormalization effect, the value of the current noise at high voltages can become even smaller than the value in the zero bias limit. We note, however, that the current is suppressed as well with the same exponent.

The dependence of the equilibrium thermal noise on T is shown in Fig. 8. Except for the vertex correction, which is irrelevant at small voltages (see below) the thermal noise is written as

$$S_{\rm th} = \frac{1}{\pi}\int d\omega\, T_{LR}(\omega)[f_L(\omega)(1-f_L(\omega)) + f_R(\omega)(1-f_R(\omega))], \tag{45}$$

with

$$T_{LR}(\omega) \equiv \Delta_L\Delta_R(\boldsymbol{G}^{\rm r})_{13}(\omega)(\boldsymbol{G}^{\rm a})_{31}(\omega). \tag{46}$$

Hence, the numerically observed power-law decay at high temperature in Fig. 8 can be understood as a renormalization of the transmission amplitude. As is shown in the figure, the thermal noise can be exactly translated into the linear conductance via the fluctuation-dissipation relation, $4GT$. This is owing to the reservoir cutoff scheme, in which the KMS condition is guaranteed.

C. The effective charge

The ratio between the noise and the current can be interpreted as an effective charge of carriers when the transport is governed by Poisson statistics [10]. On resonance, the

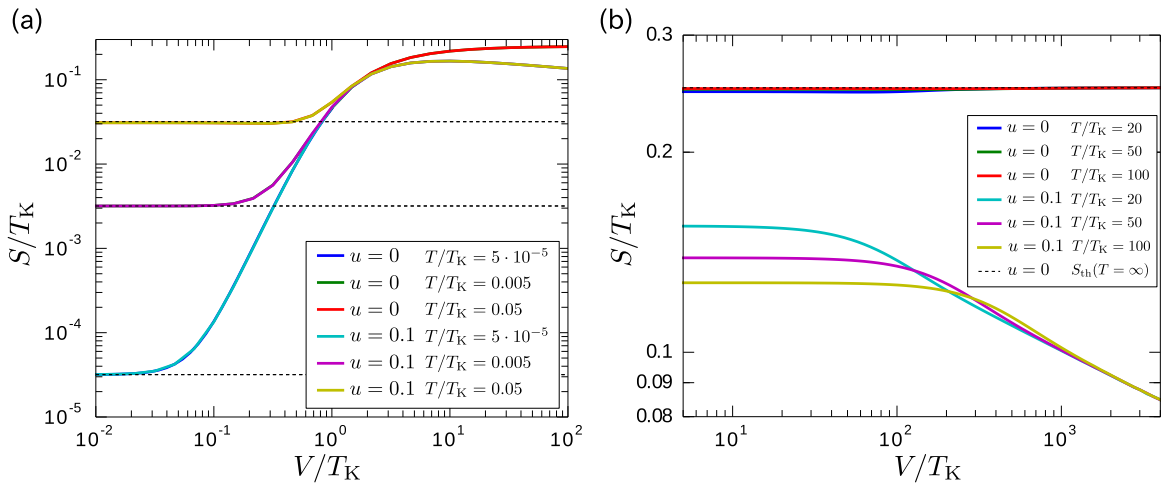

FIG. 7. The dependence of the noise on V for (a) $T < T_K$ and (b) $T > T_K$ for various u and T. The parameters are $\epsilon/T_K = 0$ and $t/\Delta = 0.001$.

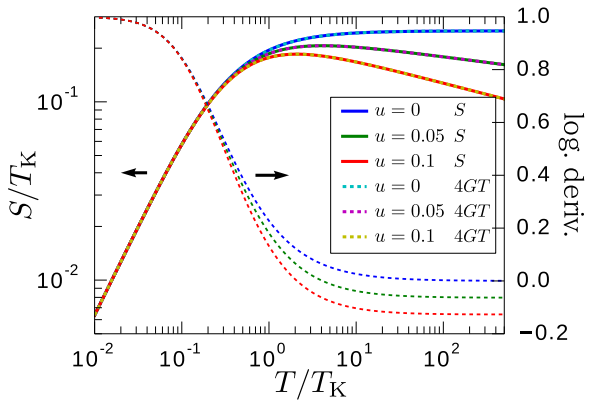

FIG. 8. The dependence of the equilibrium noise S on T for various u. The parameters are $\epsilon/T_K = 0$, $V/T_K = 0$, and $t/\Delta = 0.001$.

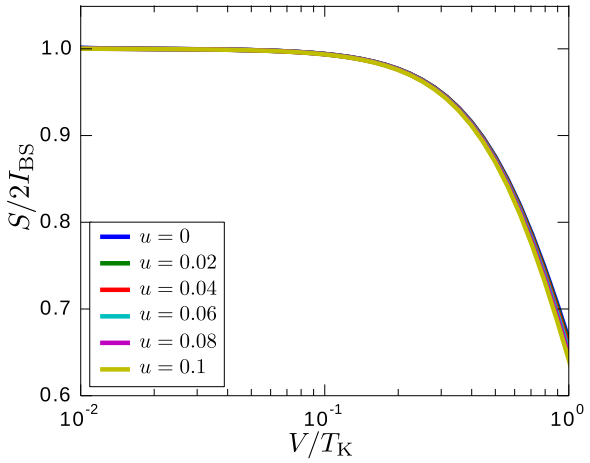

FIG. 9. The dependence of the ratio between the noise and the backscattering current on V for various u. The parameters are $\epsilon/T_K = 0$, $t/\Delta = 0.001$, and $T/T_K = 0$.

effective charge is defined as the ratio between the noise and the backscattering current [18,19]. For $u = 0$, the IRLM becomes the resonant level model and can be solved exactly. In this case, the effective charge e^* is e. Another solvable point is the self-dual one [18,19] reached at relatively large interaction. At this, field theoretical techniques and the density-matrix renormalization group approach were utilized to show that the effective charge is $2e$. It is, however, unknown, how e^* crosses over from e to $2e$ when u is increased. In this subsection, we study this issue using FRG. Since our scheme is based on an expansion in terms of the interaction strength (on the right-hand side of RG flow equations), we are bound to small-to-intermediate u.

The effective charge is defined as

$$e^* = \lim_{V\to 0} \frac{S(V)}{2I_{\rm BS}(V)}, \tag{47}$$

with the backscattering current

$$I_{\rm BS} \equiv GV - I. \tag{48}$$

The dependence of the ratio $S/2I_{\rm BS}$ on V is shown in Fig. 9 for various u. It is evident that the value of e^*/e can be reliably read off at $V/T_K = 10^{-2}$. Obviously e^* does not depend on the interaction in our approximation, from which we conclude that $e^*/e = 1 + \mathcal{O}(u^2)$ as all terms to linear order in u are kept in the truncated RG equations.

This numerical observation can be substantiated by analytic considerations. We first discuss the relation between the effective charge and the vertex correction. The transmission amplitude Eq. (46) can be expanded in terms of the bias voltage as

$$T_{\rm LR}(\omega) = T^{(0)}_{\rm LR}(\omega) - T^{(2)}_{\rm LR}(\omega)\left(\frac{V}{T_K}\right)^2 + \cdots, \tag{49}$$

in the linear-response regime ($V < T_K$). If the bias voltage is much smaller than the scale of the energy dependence of the transmission amplitude ($V \ll T_K$), the current can be evaluated at the Fermi energy as

$$\frac{I}{T_K} = \frac{1}{2\pi}\left[T^{(0)}_{\rm LR}\frac{V}{T_K} - T^{(2)}_{\rm LR}\left(\frac{V}{T_K}\right)^3\right]. \tag{50}$$

Since we are considering the on-resonance case, the zeroth-order coefficient $T^{(0)}_{LR}$ is unity. The leading term of the backscattering current is thus

$$\frac{I_{\rm BS}}{T_K} = \frac{1}{2\pi}T^{(2)}_{\rm LR}(0)\left(\frac{V}{T_K}\right)^3. \tag{51}$$

We expand the (odd) backscattering current as

$$I_{\rm BS} = G_3\left(\frac{V}{T_K}\right)^3 + G_5\left(\frac{V}{T_K}\right)^5 + \mathcal{O}\left(\left(\frac{V}{T_K}\right)^7\right). \tag{52}$$

From field theoretical considerations [31] it is known that the backscattering current is given by

$$\frac{2\pi I_{\rm BS}}{T_K} = \frac{1}{3}[1 + \mathcal{O}(u^2)]\left(\frac{V}{T_K}\right)^3 - \frac{1}{5}\left[1 - \frac{20}{3}\frac{u}{\pi} + \mathcal{O}(u^2)\right] \times \left(\frac{V}{T_K}\right)^5 + \mathcal{O}\left(\left[\frac{V}{T_K}\right]^7\right). \tag{53}$$

This analytical result can also be obtained by FRG (see endnote [52] of Ref. [31]; for a similar analysis of the current as function of temperature see Ref. [28]). By comparing the coefficients in Eq. (53) with those in Eq. (52), we find

$$\frac{G_3}{T_K} = \frac{1}{2\pi}T^{(2)}_{\rm LR}(0) = \frac{1}{6\pi}, \tag{54}$$

independent of U. We note in passing that this result can be reproduced by our numerical calculations as shown in Fig. 10(a) if T_K is properly chosen (see Appendix C). This exemplifies that our numerics gives highly accurate results and that coefficients of expansions in V/T_K can be reliably determined.

Considering the above discussion and the definition of e^*, the remaining question is whether the leading $(V/T_K)^3$ term in the current noise, S_3, has an order u correction or not. We already mentioned above that this does not seem to be the case (see Fig. 5). To analyze this further, we show the dependence of S_3 on bias voltage V in Fig. 10(b). The third-order coefficient S_3 is independent of the interaction strength

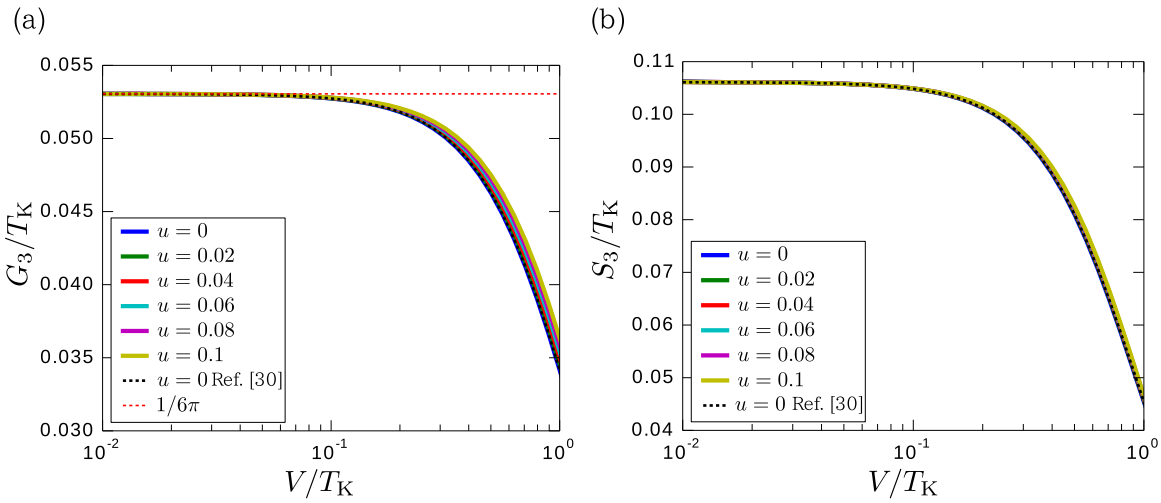

FIG. 10. (a) The dependence of the third-order coefficient of the (a) current G_3 and (b) noise S_3 on V for various u. The parameters are $\epsilon/T_K = 0$, $t/\Delta = 0.001$, and $T/T_K = 0$.

at low bias voltages, which is consistent with the result of e^*/e shown in Fig. 9.

In the subsequent discussion, we give a microscopic explanation of the u independence of the third-order coefficient, S_3, by dividing the noise into the bubble term and the vertex correction. If we denote the bubble and vertex correction terms by $S_0 \equiv S^0_{LL}(\omega = 0)$ and $S_U \equiv S^U_{LL}(\omega = 0)$, respectively, the current noise can be written as

$$S = S_0 + S_U. \tag{55}$$

At zero-temperature, the bubble term is given as

$$S_0 = \frac{1}{\pi}\int_{-V/2}^{V/2} d\omega\, T_{LR}(\omega)[1 - T_{LR}(\omega)]. \tag{56}$$

If we ignore the frequency dependence of the transmission amplitude, we obtain

$$\frac{S_0}{T_K} = \frac{1}{\pi}\frac{V}{T_K} T_{LR}(0)[1 - T_{LR}(0)]. \tag{57}$$

Since we are considering the on-resonance case $[T^{(0)}_{\rm LR}(0) = 1]$, the contribution linear in V to the bubble term vanishes. The lowest order contribution in V is thus

$$\begin{aligned}\frac{S_0}{T_K} &= \frac{1}{\pi}\left(\frac{V}{T_K}\right)^3 T^{(2)}_{\rm LR}(0)\left[2T^{(0)}_{\rm LR}(0) - 1\right]\Big|_{T^{(0)}_{LR}(0)=1} \\ &= \frac{1}{\pi}\left(\frac{V}{T_K}\right)^3 T^{(2)}_{\rm LR}(0).\end{aligned} \tag{58}$$

With this, the effective charge is obtained as

$$e^* = \left.\frac{S}{2I_{\rm BS}}\right|_{V=0} = 1 + \left.\frac{S_U}{2I_{\rm BS}}\right|_{V=0} = 1 + \left.\frac{3\pi S_U}{(V/T_K)^3}\right|_{V=0}. \tag{59}$$

This relation shows that the U dependence of the effective charge is incorporated via the vertex correction S_U analyzed next.

The current-vertex functions enter the expression for the vertex correction S_U [see Eq. (17)]. The three-point vertex function can be computed in two different ways by either plain perturbation theory or by solving its flow equations (27) and (30). It is well established that the self-energy computed in leading order perturbation theory in u is plagued by a logarithmically divergent term [6]. To avoid this known problem in a perturbative computation of S_U, depicted in the right diagram of Fig. 2, we dressed the two propagators by the self-energy computed within FRG. This way we single out possible problems of a perturbative calculation of the three-point vertex function itself. The dependence of S_U on V obtained by perturbation theory and FRG is shown in Fig. 11 for different t/Δ. In both computations, the vertex correction scales as V^4 for small V, which is subleading compared with the bubble term which goes as V^3. A significant difference is that the results obtained by perturbation theory becomes gradually larger the deeper one goes into the scaling limit $t/\Delta \ll 1$. The vertex corrections calculated using FRG for the three-point vertex are free of this problem and collapse into a single curve if rescaled by T_K. This indicates that, in analogy to the self-energy, the FRG regularizes the divergences of the vertex correction.

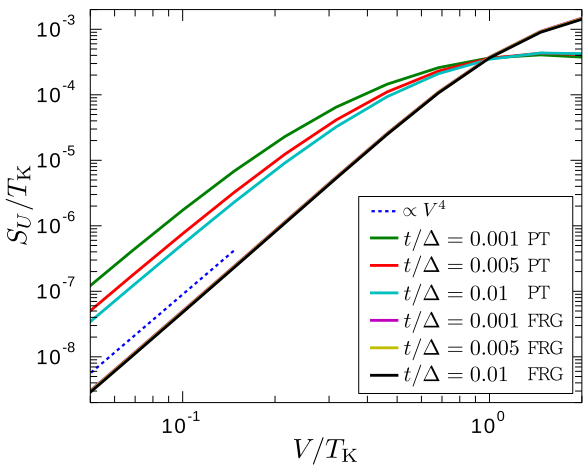

FIG. 11. The vertex correction calculated using a FRG scheme and a plain perturbation theory for various t as a function of V. The parameters are $u = 0.1$, $\epsilon/T_K = 0$, and $T/T_K = 0$.

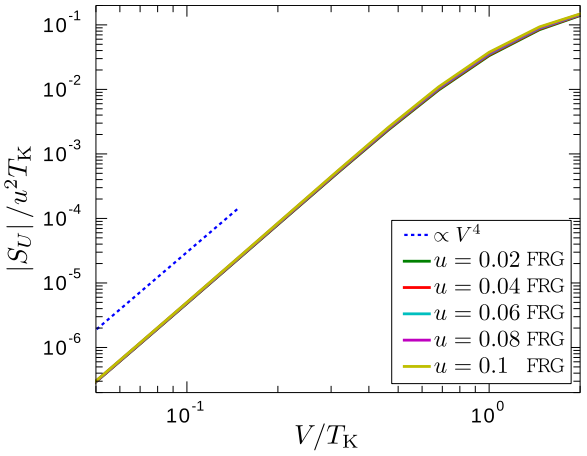

FIG. 12. The vertex correction divided by u^2 calculated using our FRG scheme for various u as a function of V. The parameters are $\epsilon/T_K = 0$, $t/\Delta = 0.001$, and $T/T_K = 0$.

The vertex correction fully computed by FRG and divided by u^2 is plotted for various u in Fig. 12. From this figure, it is evident that S_U depends on u and V as $|S_U|/T_K \propto u^2(V/T_K)^4$. Because of the u^2 prefactor in the linear response regime ($V < T_K$), the vertex correction is not under control within the static approximation which only contains all terms to order u. However, the vertex correction does not contribute to the effective charge because it is of order V^4 while the bubble term scales as V^3 [see Eq. (59)].

D. Off-resonance current noise

In this subsection, we investigate the current noise away from the particle-hole symmetric point ($\epsilon \neq 0$). We start out by considering the current noise with the three-point vertex functions calculated using plain perturbation theory, but with all propagators dressed by the FRG self-energy (see above). The noise as a function of voltage for different u and t/Δ is shown in Fig. 13(a). If the level energy aligns with one of the leads chemical potentials ($\epsilon \sim \pm V/2$) a peak develops. The peak exhibits divergent behavior for decreasing t/Δ, that is, when going into the scaling limit, at fixed u. We reemphasize that this divergence originates from the vertex function, as logarithmic divergences of the self-energy have already been removed by employing the FRG self-energy. The vertex correction to the noise S_U divided by u is shown in Fig. 13(b). From this we conclude that the term diverging for $t/\Delta \to 0$ has a prefactor u. Plain perturbation theory can thus not be used to study the current noise away from particle-hole symmetry in the scaling limit even for very small u.

The current noise and its vertex correction determined by our FRG scheme are shown in Fig. 14. The vertex functions are obtained by solving their flow equations Eqs. (27) and (30). The divergent behavior of the current noise observed in Fig. 13(a) is essentially removed for the curves in Fig. 14(a). Further down we comment on the weak features still visible in the regime $\epsilon \sim \pm V/2$. This indicates that, as for the self-energy (and thus the current when employing the Meir-Wingreen formula), the RG-based scheme regularizes the leading-order divergences. To further analyze this the vertex correction to the noise S_U divided by u^2 is shown in Fig. 14(b). This figure indicates that the divergence with prefactor u of first order perturbation theory [see Fig. 13(b)] is pushed to order u^2 within FRG. As our truncation does not contain all terms $\mathcal{O}(u^2)$ we do not control S_U to this order. This second-order divergence in S_U manifests as the artificial dip of the noise for $u = 0.02$ and $t/\Delta = 0.001$ and the shoulders for the other parameter sets found in Fig. 14(a). When next considering larger interactions we thus take $t/\Delta = 0.01$ instead of 0.001 as before to avoid this order u^2 artifact.

The current noise as a function of V is shown in Fig. 15 for a variety of u. The current noise is proportional to V in the linear-response regime (see the plot for $V < T_K$ as well as the analytic considerations in Sec. III C). At large bias voltages, the current crosses overs to a power-law decay with an interaction-dependent exponent. The exponent agrees with the one found for $\epsilon = 0$: $\alpha_S = -4u/\pi$. This is in accordance with our intuition that the bias voltage dominates the transport for $V \gg \epsilon$.

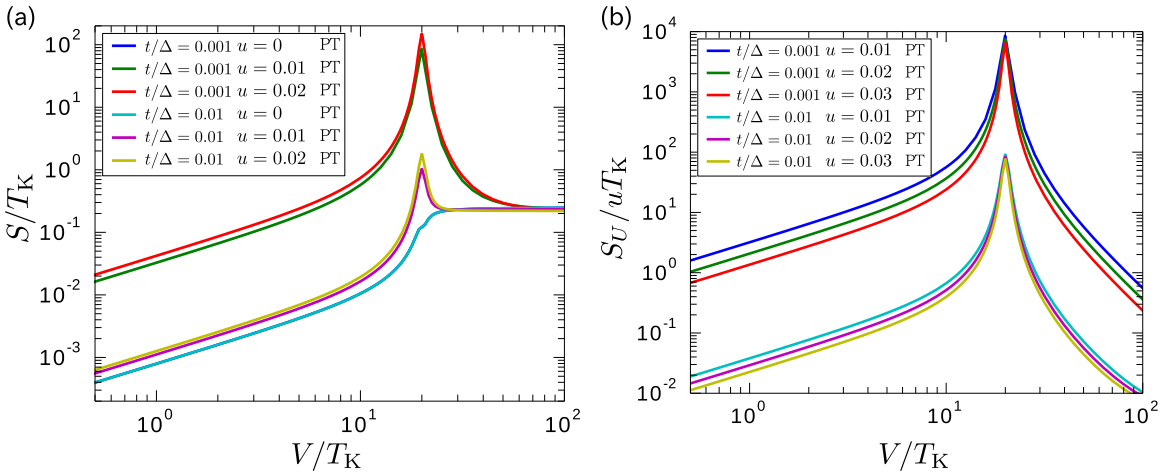

FIG. 13. (a) The current noise and (b) the vertex correction calculated from a plain perturbation theory for various u and t away from the particle-hole symmetric point as a function of V. The parameters are $\epsilon/T_K = 10$ and $T/T_K = 0$.

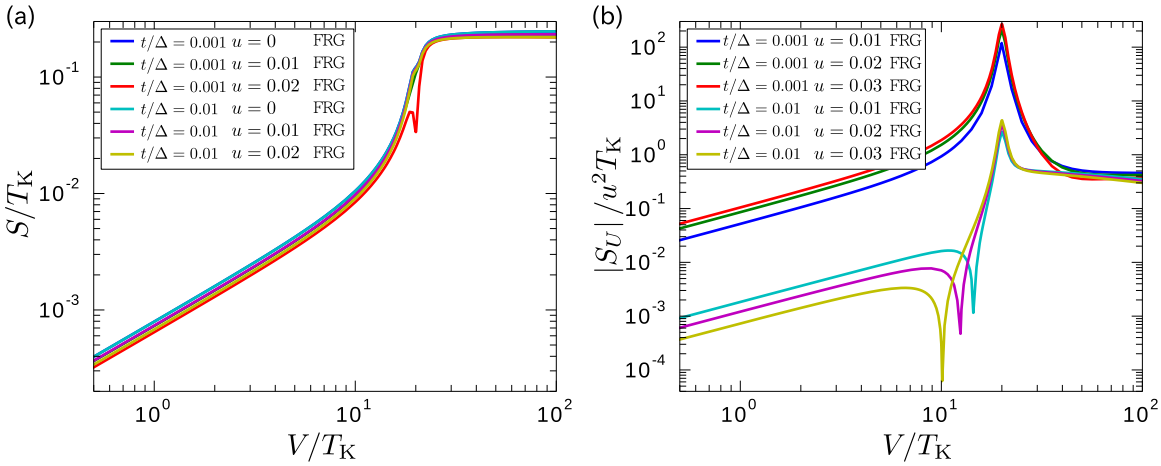

FIG. 14. (a) The current noise and (b) the vertex correction divided by u^2 calculated using our FRG scheme for various u and t away from the particle-hole symmetric point as a function of V. The parameters are $\epsilon/T_K = 10$ and $T/T_K = 0$.

The dependence of the current noise on ϵ at fixed V is shown in Fig. 16. It is independent of ϵ for $\epsilon \ll V$ as the level is placed inside the bias window. The noise starts to decrease when the level energy is beyond the bias window ($\epsilon \gtrsim V/2$). The weak features found when the level is aligned with one of the lead chemical potentials were discussed above. For large $\epsilon \gg T_K$, the noise crosses over to a power-law decay as a function of ϵ as the renormalization of the hoping amplitude is cut by the level position in this case. For $u = 0$ the exponent is -2 and the interacting part of the exponent is found to be twice that of the V dependence; see the logarithmic derivative shown in Fig. 16 for $\epsilon/T_K \leqslant 1$ and $\epsilon/T_K \geqslant 10$.

IV. SUMMARY

In the present paper, we have developed a FRG scheme to describe the current noise of the nonequilibrium IRLM. The coupled set of flow equations of the current-vertex functions and the self-energy are derived and solved to determine the current noise within the lowest-order approximation in the two-particle interaction.

The vertex correction of the current noise shows divergent behavior in the scaling limit, if it is calculated using plain perturbation theory. This divergence is removed in our FRG method at the particle-hole symmetric point, which makes it possible to perform a reliable analysis in the deep scaling limit. In this regime, the current noise is found to show a power-law decay at high voltages characterized by the same exponent as that of the current. This property is robust against temperature. The effective charge of the IRLM at the particle-hole symmetric point can be reliably extracted and is found to be interaction independent to linear order. This behavior can be understood from the properties of the vertex contribution to the noise by combining analytical arguments and the numerical results.

The current noise away from the particle-hole symmetric point determined by plain perturbation theory shows a severe leading order divergence, which originates from the current-vertex correction. We showed that the divergent term which is proportional to u is consistently removed in our scheme and pushed to order u^2; this lies beyond our control. Although the remaining order u^2 divergence is an obstacle to calculate the current noise for the particle-hole asymmetric case in the

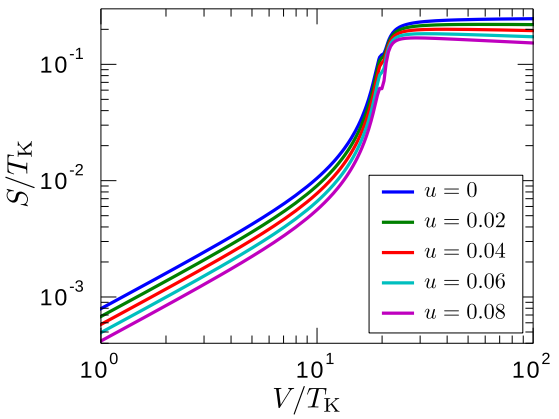

FIG. 15. The dependence of the current noise on V for various u away from the particle-hole symmetric point. The parameters are $\epsilon/T_K = 10$, $t/\Delta = 0.01$, and $T/T_K = 0$.

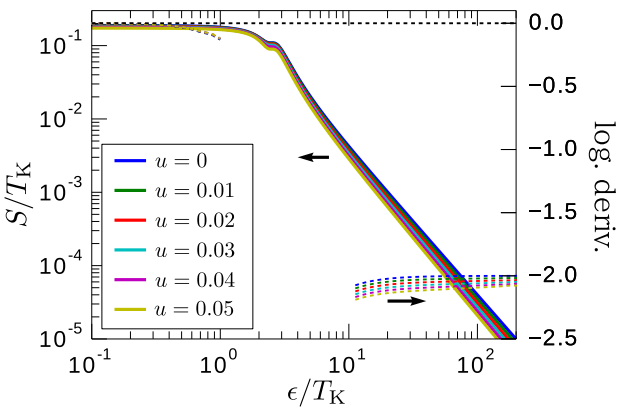

FIG. 16. The dependence of the current noise and its logarithmic derivative on ϵ for various u. The parameters are $V/T_K = 5$, $t/\Delta = 0.01$, and $T/T_K = 0$.

scaling limit ($t/\Delta \ll 1$), we obtain reliable results down to $t/\Delta = 0.01$. We showed that the current noise shows a power-law decay for $\max\{V,\epsilon\} \gg T_{\rm K}$.

The present paper shows that the FRG method allows one to reliably calculate the current noise in the scaling regime. A higher order FRG calculation—possible in principle, complicated in practice—would be desirable to further elucidate the crossover of the effective charge from the noninteracting case ($e^*/e = 1$) to the self-dual point ($e^*/e = 2$) at relatively large u. Furthermore, the higher order contributions need to be taken into account in order to remove a diverging term of order u^2 away from particle-hole symmetry and discuss the current noise in the deep scaling limit for this case. Another step for the future would be to extend the FRG treatment to determine the full counting statistics of interacting fermion systems.

ACKNOWLEDGMENTS

We thank Takeo Kato, Akinori Nishino, Katharina Eissing, and Peter Schmitteckert for very useful discussions. T.J.S. acknowledges financial support provided by the Advanced Leading Graduate Course for Photon Science (ALPS). This work was supported by the Deutsche Forschungsgemeinschaft via RTG 1995.

APPENDIX A: INITIAL CONDITIONS

The initial condition of the self-energy for $\Lambda_{\rm init} \to \infty$ is written as

$$\left(\mathbf{\Sigma}^{\rm r}_{U,\Lambda_{\rm init}}\right)_{11}(\omega) = U_1 n_2, \tag{A1}$$

$$\left(\mathbf{\Sigma}^{\rm r}_{U,\Lambda_{\rm init}}\right)_{22}(\omega) = U_1 n_1 + U_3 n_3, \tag{A2}$$

$$\left(\mathbf{\Sigma}^{\rm r}_{U,\Lambda_{\rm init}}\right)_{33}(\omega) = U_3 n_2, \tag{A3}$$

$$\left(\mathbf{\Sigma}^{\rm K}_{U,\Lambda_{\rm init}}\right)_{ij}(\omega) = 0, \tag{A4}$$

where n_i is the occupation of the ith site.

By a simple diagrammatic argument [23], current-vertex functions are found to be identical to those of the noninteracting system in the limit of $\Lambda_{\rm init} \to \infty$;

$$\left(\boldsymbol{\gamma}^{(2,n)}_{\Lambda_{\rm init}}\right)^{\nu_1';{\rm s}\cdots{\rm s}}_{ij;\alpha_1\cdots\alpha_n}(t_1',t_1;t_1''\cdots t_n'') = \left(\boldsymbol{\gamma}^{(2,n)}_{\rm res}\right)^{\nu_1';{\rm s}\cdots{\rm s}}_{ij;\alpha_1\cdots\alpha_n}(t_1',t_1;t_1''\cdots t_n'') \quad (\text{for } n>0). \tag{A5}$$

The noninteracting current-vertex functions can be determined using the Ward-Takahashi identity

$$\left(\boldsymbol{\gamma}^{(2,1)}_{\rm res}\right)_{11;L}(\tau',\tau;\tau'') = i[\delta(\tau',\tau'') - \delta(\tau,\tau'')](\mathbf{\Sigma}_{\rm res})_{11}(\tau',\tau). \tag{A6}$$

The other components of the three-point vertex functions are zero because the source field $A_L(\tau)$ is only included in the (1,1) component of the tunneling self-energy Eq. (5). The initial conditions of the three-point current-vertex functions are obtained as

$$\left(\boldsymbol{\gamma}^{(2,1)}_{\Lambda_{\rm init}}\right)^{\rm r;s}_{ij;\alpha_1}(\omega_1,\omega_1;0) = -\delta_{i1}\delta_{j1}\delta_{\alpha_1 L}\Delta_L(1-2f_L(\omega_1)), \tag{A7}$$

$$\left(\boldsymbol{\gamma}^{(2,1)}_{\Lambda_{\rm init}}\right)^{\rm a;s}_{ij;\alpha_1}(\omega_1,\omega_1;0) = \delta_{i1}\delta_{j1}\delta_{\alpha_1 L}\Delta_L(1-2f_L(\omega_1)), \tag{A8}$$

$$\left(\boldsymbol{\gamma}^{(2,1)}_{\Lambda_{\rm init}}\right)^{\rm K;s}_{ij;\alpha_1}(\omega_1,\omega_1;0) = -\delta_{i1}\delta_{j1}\delta_{\alpha_1 L}\Delta_L, \tag{A9}$$

$$\left(\boldsymbol{\gamma}^{(2,1)}_{\Lambda_{\rm init}}\right)^{\tilde{\rm K};{\rm s}}_{ij;\alpha_1}(\omega_1,\omega_1;0) = \delta_{i1}\delta_{j1}\delta_{\alpha_1 L}\Delta_L. \tag{A10}$$

Here, we show only the case with $\omega_1 = \omega_1'$ because we focus on the zero-frequency current noise in this paper. We note that $\left(\boldsymbol{\gamma}^{(2,1)}_{\Lambda_{\rm init}}\right)^{\tilde{\rm K};{\rm s}}$ does not need to be zero. The multipoint current vertices are determined by recursively using the Ward-Takahashi identity, and the initial conditions for four-point current-vertex functions are

$$\left(\boldsymbol{\gamma}^{(2,2)}_{\Lambda_{\rm init}}\right)^{\rm r;ss}_{ij;\alpha_1\alpha_2}(\omega_1,\omega_1;0,0) = 2i\delta_{i1}\delta_{j1}\delta_{\alpha_1 L}\delta_{\alpha_2 L}\Delta_L, \tag{A11}$$

$$\left(\boldsymbol{\gamma}^{(2,2)}_{\Lambda_{\rm init}}\right)^{\rm a;ss}_{ij;\alpha_1\alpha_2}(\omega_1,\omega_1;0,0) = -2i\delta_{i1}\delta_{j1}\delta_{\alpha_1 L}\delta_{\alpha_2 L}\Delta_L, \tag{A12}$$

$$\left(\boldsymbol{\gamma}^{(2,2)}_{\Lambda_{\rm init}}\right)^{\rm K;ss}_{ij;\alpha_1\alpha_2}(\omega_1,\omega_1;0,0) = 2i\delta_{i1}\delta_{j1}\delta_{\alpha_1 L}\delta_{\alpha_2 L} \times \Delta_L(1-2f_L(\omega_1)), \tag{A13}$$

$$\left(\boldsymbol{\gamma}^{(2,2)}_{\Lambda_{\rm init}}\right)^{\tilde{\rm K};{\rm ss}}_{ij;\alpha_1\alpha_2}(\omega_1,\omega_1;0,0) = -2i\delta_{i1}\delta_{j1}\delta_{\alpha_1 L}\delta_{\alpha_2 L} \times \Delta_L(1-2f_L(\omega_1)). \tag{A14}$$

The initial conditions of the four-point and higher-point vertex functions are determined by the bare action. If we denote the antisymmetrized bare two-particle interaction [32] by $U_{ij;kl}$, these vertex functions are written as

$$\left(\boldsymbol{\gamma}^{(4,0)}_{\Lambda_{\rm init}}\right)^{\nu_1'\nu_2';\nu_1\nu_2}_{ij;kl}(\omega_1',\omega_2';\omega_1,\omega_1'+\omega_2'-\omega_1) = \begin{cases} -\nu_1' U_{ij;kl} & \text{if } \nu_1' = \nu_2' = \nu_1 = \nu_2, \\ 0 & \text{otherwise.} \end{cases} \tag{A15}$$

$$\left(\boldsymbol{\gamma}^{(4,m)}_{\Lambda_{\rm init}}\right)^{\nu_1'\nu_2';\nu_1\nu_2;\nu_1''\cdots\nu_m''}_{ij;kl;\alpha_1\cdots\alpha_m}(\omega_1',\omega_2';\omega_1,\omega_2;\omega_1'',\ldots,\omega_m'') = 0 \quad (m>0). \tag{A16}$$

APPENDIX B: NUMERICAL DETAILS

For the plots in the main text, we take the error of solving the set of ordinary differential equations to be $10^{-6}T_{\rm K}$. The frequency grid points are determined using geometric sequences with a scale factor $\Delta\omega = 10^{-8}T_{\rm K}$. The number of the grid points is $N_{\rm grid} = 4801$, which is sufficient to produce $N_{\rm grid}$ independent results. As our main interest lies in the scaling regime, the band width Δ should be taken to be large enough for the t/Δ correction to be negligible. We used $\Delta = 10^4$ and 10^6 for $t/\Delta = 0.01$ and 0.001, respectively.

APPENDIX C: DEFINITION OF $T_{\rm K}$

Several ways exist to define the emergent low-energy scale $T_{\rm K}$. Within the FRG approach the most natural ones are either by the renormalized hopping amplitude or the susceptibility. We used the renormalized hopping amplitude in the main text. The other definition utilized in previous FRG works is

$$T_{\rm K}^{\rm sus} \equiv -\frac{2}{\pi}\left(\left.\frac{d\langle n_2\rangle}{d\epsilon}\right|_{T=V=\epsilon=0}\right)^{-1}, \tag{C1}$$

where $\langle n_2 \rangle$ is the occupation of the quantum dot site 2. Deep in the scaling regime both definitions can equivalently be used when comparing with field theoretical results obtained for $t/\Delta \to 0$. We found that, for the t/Δ reachable by us, results rescaled with the T_K derived from the renormalized hopping show weaker t/Δ corrections and are thus closer to the field theoretical predictions. For this reason we used this definition in the main text.

[1] P. Schlottmann, Phys. Rev. B **25**, 4815 (1982).
[2] B. Doyon, Phys. Rev. Lett. **99**, 076806 (2007).
[3] L. Borda, K. Vladár, and A. Zawadowski, Phys. Rev. B **75**, 125107 (2007).
[4] E. Boulat, H. Saleur, and P. Schmitteckert, Phys. Rev. Lett. **101**, 140601 (2008).
[5] A. Nishino, T. Imamura, and N. Hatano, Phys. Rev. Lett. **102**, 146803 (2009).
[6] C. Karrasch, M. Pletyukhov, L. Borda, and V. Meden, Phys. Rev. B **81**, 125122 (2010).
[7] C. Karrasch, S. Andergassen, M. Pletyukhov, D. Schuricht, L. Borda, V. Meden, and H. Schoeller, Europhys. Lett. **90**, 30003 (2010).
[8] S. Andergassen, M. Pletyukhov, D. Schuricht, H. Schoeller, and L. Borda, Phys. Rev. B **83**, 205103 (2011).
[9] A. Nishino, N. Hatano, and G. Ordonez, Phys. Rev. B **91**, 045140 (2015).
[10] Y. Blanter and M. Büttiker, Phys. Rep. **336**, 1 (2000).
[11] L. Saminadayar, D. C. Glattli, Y. Jin, and B. Etienne, Phys. Rev. Lett. **79**, 2526 (1997); R. De-Picciotto, M. Reznikov, M. Heiblum, V. Umansky, G. Bunin, and D. Mahalu, Nature (London) **389**, 162 (1997).
[12] F. Lefloch, C. Hoffmann, M. Sanquer, and D. Quirion, Phys. Rev. Lett. **90**, 067002 (2003).
[13] Y. Yamauchi, K. Sekiguchi, K. Chida, T. Arakawa, S. Nakamura, K. Kobayashi, T. Ono, T. Fujii, and R. Sakano, Phys. Rev. Lett. **106**, 176601 (2011).
[14] M. Ferrier, T. Arakawa, T. Hata, R. Fujiwara, R. Delagrange, R. Weil, R. Deblock, R. Sakano, A. Oguri, and K. Kobayashi, Nat. Phys. (2015).
[15] S. Hershfield, Phys. Rev. B **46**, 7061 (1992).
[16] A. Golub, Phys. Rev. B **76**, 193307 (2007).
[17] P. Fendley, A. W. W. Ludwig, and H. Saleur, Phys. Rev. B **52**, 8934 (1995).
[18] A. Branschädel, E. Boulat, H. Saleur, and P. Schmitteckert, Phys. Rev. Lett. **105**, 146805 (2010).
[19] S. T. Carr, D. A. Bagrets, and P. Schmitteckert, Phys. Rev. Lett. **107**, 206801 (2011).
[20] S. T. Carr, P. Schmitteckert, and H. Saleur, Phys. Scr. **T165**, 014009 (2015).
[21] W. Metzner, M. Salmhofer, C. Honerkamp, V. Meden, and K. Schönhammer, Rev. Mod. Phys. **84**, 299 (2012).
[22] S. G. Jakobs, M. Pletyukhov, and H. Schoeller, J. Phys. A: Math. Theor. **43**, 103001 (2010).
[23] S. G. Jakobs, M. Pletyukhov, and H. Schoeller, Phys. Rev. B **81**, 195109 (2010).
[24] A. Kamenev, *Field Theory of Non-Equilibrium Systems* (Cambridge University Press, Cambridge, 2011).
[25] K. Chou, Z. Su, B. Hao, and L. Yu, Phys. Rep. **118**, 1 (1985).
[26] G.-H. Ding and B. Dong, Phys. Rev. B **87**, 235303 (2013).
[27] D. M. Kennes, S. G. Jakobs, C. Karrasch, and V. Meden, Phys. Rev. B **85**, 085113 (2012).
[28] D. M. Kennes and V. Meden, Phys. Rev. B **87**, 075130 (2013).
[29] Y. Meir and N. S. Wingreen, Phys. Rev. Lett. **68**, 2512 (1992).
[30] A. Branschädel, E. Boulat, H. Saleur, and P. Schmitteckert, Phys. Rev. B **82**, 205414 (2010).
[31] L. Freton and E. Boulat, Phys. Rev. Lett. **112**, 216802 (2014).
[32] J. W. Negele and H. Orland, *Quantum Many-Particle Systems* (Westview, Bouldeer, CO, 1988).